ISSN 1063-7834, Physics of the Solid State, 2013, Vol. 55, No. 6, pp. 1214–1219. © Pleiades Publishing, Ltd., 2013.
Original Russian Text © V.A. Vazhenin, A.P. Potapov, A.V. Fokin, M.Yu. Artyomov, 2013, published in Fizika Tverdogo Tela, 2013, Vol. 55, No. 6, pp. 1126–1131.

IMPURITY CENTERS

Electron Paramagnetic Resonance of Gd^{3+} Ions in $Ca_{1-x-y}Y_xGd_yF_{2+x+y}$ Crystals

V. A. Vazhenin[a, *], A. P. Potapov, A. V. Fokin, and M. Yu. Artyomov

Institute of Physics and Applied Mathematics, Ural Federal University named after the First President of Russia B.N. Yeltsin, pr. Lenina 51, Yekaterinburg, 620000 Russia

** e-mail: vladimir.vazhenin@usu.ru*

Received November 22, 2012

Abstract—Electron paramagnetic resonance of $Ca_{1-x-y}Y_xGd_yF_{2+x+y}$ single crystals has revealed spectra that are not typical of gadolinium-doped CaF_2 crystals. These spectra have a nearly tetragonal symmetry and are most probably caused by Gd^{3+} ions localized in yttrium clusters. Weak spectra of tetragonal Gd^{3+} centers, whose parameters are close to those of a cubic gadolinium center caused by an isolated Gd^{3+} ion, have been also detected. These centers are attributed to isolated Gd^{3+} ions localized near octahedral rare-earth clusters or their associations.

DOI: 10.1134/S1063783413060322

1. Doping of alkaline-earth fluorides MF_2 (M = Ca, Cd, Sr, Ba) with a fluorite structure by trivalent ions R (R are the rare-earth, yttrium or scandium, ions) with a concentration of more than 0.1 mol % leads to the formation of detectable rare-earth clusters in the crystal, which include the groups of interstitial fluorine ions and are coherently conjugate with the host lattice [1, 2].

Two types of cluster structures are most known in MF_2–RF_3 solid solutions. In the first one, the octahedron composed of 6 R and M ions in cationic positions embraces a cuboctahedron of 12 anions situated at the edges of the initial fluorine cube [1–8], and therefore the nearest neighborhood of the $R(M)$ ion is a square antiprism or a Thomson cube (Fig. 1). Such an octahedral cluster $[R_{6-x}M_xF_{36}]$ or the cluster $[R_{6-x}M_xF_{37}]$, which includes a fluorine ion situated inside the anionic cuboctahedron, substitutes the fragment $[M_6F_{32}]$ of the regular structure of fluorite thus weakly distorting the lattice. The presence of M ions in the rare-earth octahedron provides electroneutrality of the cluster. Larger structural elements, the $\{M_8[R_6F_{68}]\}$ and $\{M_8[R_6F_{69}]\}$ superclusters, which include the above octahedral clusters, are the minimum cubic parts of the crystal containing all types of structural defects.

Another most known type of clusters, tetrahedral one, includes 4 R and M ions in cationic positions and the tetrahedron of interstitial F^- ions around the central fluorine vacancy (see Fig. 1 in [2]). This cluster is described by the formula $[M_{4-x}R_xF_{26}]$ and substitutes the lattice fragment $[M_4F_{23}]$ [9].

The formation of the octahedral or tetrahedral cluster depends primarily on the ratio of the ionic radii of different-valence isomorphously substituted cations M^{2+} and R^{3+}: the formation of tetrahedral clusters is more probable at $r(R^{3+})/r(M^{2+}) > 0.95$ [9–14].

By the analysis of the magnetic resonance spectra of Er^{3+}, Tm^{3+}, and Yb^{3+} in yttrium- and lutetium-doped CaF_2, SrF_2, and BaF_2 crystals, Kazanskii et al. [5–8] found that paramagnetic rare-earth ions are localized in octahedral yttrium or lutetium clusters. In addition, these paramagnetic ions, whose spectra have predominantly tetragonal symmetry, exhibit a considerable scatter in the principal axes of g tensor.

Tetrahedral rare-earth clusters in cadmium fluoride crystals were studied in [10–14]. It was found by X-ray diffraction analysis of $Cd_{0.9}R_{0.1}F_{2.1}$ (R = Y, Er, Tm, Lu, Yb, Gd, Ho) crystals that they predominantly form tetrahedral $[R_2Cd_2F_{26}]$ clusters and an excessive negative charge is compensated by fluorine vacancies [10, 11]. However, studying the conductivity of these

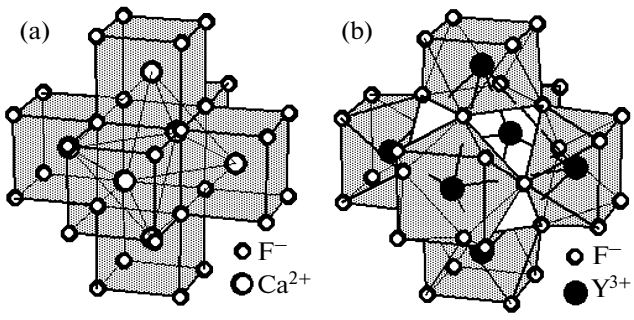

Fig. 1. (a) $[Ca_6F_{32}]$ fragment of the fluorite lattice and (b) the structure of the $[Y_6F_{37}]$ octahedral cluster [6].

crystals, Sorokin et al. [12] came to the conclusion that ionic transport in $Cd_{0.9}R_{0.1}F_{2.1}$ is caused by interstitial fluorine ions outside the clusters. This witnesses in favor of a higher probability of the formation of $[R_4F_{26}]$ clusters. In our previous works [13, 14], using electron paramagnetic resonance (EPR), we succeeded to discover three types (C_{3V} and two C_S) high-spin Gd^{3+} centers localized in tetrahedral yttrium–gadolinium clusters.

The possibility of forming the inverted octahedral supercluster $\{R_8[M_6F_{69}]\}$ with a cuboctahedral anionic group in the case of large rare-earth ions was discussed in [15].

As a result of studying $Ba_{0.75}Lu_{0.25}F_{2.25}$ crystals [16], one more defect complex was proposed—the supercluster $\{R_8[Ba_6F_{71}]\}$, which is structurally close to the fragment $[M_{14}F_{64}]$ and different from the rare-earth supercluster $\{Ba_8[R_6F_{68,69}]\}$ in that its core is formed by alkaline-earth ions forming $[BaF_{10}]$ polyhedra, rather than by rare-earth ions.

In addition, linear clusters oriented along the trigonal axis and composed of rare-earth and interstitial fluorine ions were observed in $Ba_{1-x}La_xF_{2+x}$:Yb^{3+} [17, 18].

This work is devoted to the EPR investigation of high-spin gadolinium centers in calcium fluoride crystals with an impurity of nonmagnetic yttrium ions.

2. We studied CaF_2 single crystals with 0.1 mol % of GdF_3; some samples were doped with 3 mol % of yttrium trifluoride. At this concentration ratio of the impurity cations Gd^{3+} and Y^{3+}, most probable is the existence of yttrium clusters with or without one Gd^{3+} ion. The measurements were carried out at room temperature and at 180 K on a Bruker EMX Plus X-band EPR spectrometer and a modified RE-1301 spectrometer.

3. Transformation of the EPR spectrum of gadolinium in CaF_2 and CdF_2 due to yttrium doping is described in detail elsewhere [19]. The spectra of both $Ca_{1-x-y}Y_xGd_yF_{2+x+y}$ and $Cd_{1-x-y}Y_xGd_yF_{2+x+y}$ single crystals [13, 14] exhibit an intense Gd^{3+} cubic center (Fig. 2) caused by individual gadolinium ions, whose parameters of the spin Hamiltonian within the experimental error coincide with those of the cubic centers in yttrium-free crystals [19].

In addition, the EPR spectrum of $Ca_{1-x-y}Y_xGd_yF_{2+x+y}$ exhibits the signals (Fig. 2) of tetragonal $Gd^{3+}-F_i^-$ dimer centers (F_i^- is an interstitial fluorine ion), whose intensity relative to the signal of cubic centers is much lower than in CaF_2. There is almost no effect of yttrium impurity in the crystal on the parameters of the spin Hamiltonian of the $Gd^{3+}-F_i^-$ dimer centers (Table 1). The presence of such cubic and dimer gadolinium centers in $Ca_{1-x-y}Y_xGd_yF_{2+x+y}$ witnesses convincingly the existence of the regions with a nearly undistorted fluorite structure in the crystals.

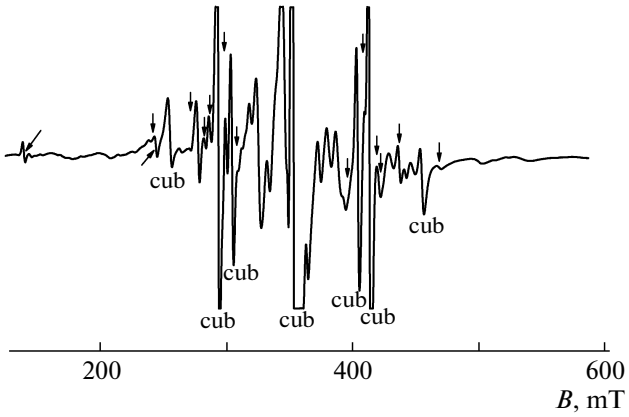

Fig. 2. EPR spectrum (first derivative of absorption signals) of $Ca_{1-x-y}Y_xGd_yF_{2+x+y}$ in the magnetic field $\mathbf{B} \parallel \mathbf{C}_4$ ($\mathbf{B}$ is the magnetic field induction) at $T = 300$ K and a frequency of 9.87 GHz. Vertical and tilted arrows mark the satellites of the signals from the Gd^{3+} cubic center and the signals from the $Gd^{3+}-F_i^-$ tetragonal dimer centers, respectively.

The EPR spectrum of the $Ca_{1-x-y}Y_xGd_yF_{2+x+y}$ samples has the maximum width (~400 mT) at $\mathbf{B} \parallel \mathbf{C}_4$ (Fig. 2).[1] The resonance positions of the majority of the spectral components (first of all, of the peripheral ones) have extreme values at this orientation. These features of the spectrum are typical for the centers of predominantly tetragonal symmetry, in agreement with the earlier results [5–8].

The signals detected in the central part of the spectrum are largely the superpositions of several transitions, which prevents obtaining adequate information on the orientation behavior of individual signals. A large number of transitions in the central part of the spectrum can be explained by the existence of three types of octahedral yttrium–gadolinium clusters (Table 2) with 6 different kinds of paramagnetic Gd^{3+} centers of tetragonal and lower (C_{2V}, C_S) symmetry. A difference in structure and electric charge between different types of clusters (Table 2) is caused by the numbers of R and M ions entering these clusters [10, 11]. The paramagnetic center with the local symmetry indicated in Table 2 is a Gd^{3+} ion in the cationic position of the cluster with a certain mutual position of other cations. Magnetic multiplicity is the number of equivalent paramagnetic centers with different orientations.

Similar data are presented in Table 2 for tetrahedral rare-earth clusters that appear in $Cd_{1-x}Y_xF_{2+x}$

[1] The $Ca_{1-y}Gd_yF_{2+y}$ samples do not feature such an EPR spectrum.

Table 1. Parameters of the spin Hamiltonian of tetragonal $Gd^{3+}-F_i^-$ centers (the standard deviation f and the parameters b_{nm} are given in MHz)

Parameter	$CaF_2:Gd^{3+}$ [20]	$CaF_2:Gd^{3+}$ (this work)	$Y_xCa_{1-x}F_{2+x}:Gd^{3+}$ (this work)
g	1.992(1)	1.992	1.992
b_{20}	−4452(3)	−4443	−4435
b_{40}	−69.3(3)	−71	−75
b_{44}	−441(3)	−433	−415
b_{60}	−2.1(3)	−3	−6
b_{64}	16(1)	30	44
f		13	35

crystals. As is seen, the situation with the variety of Gd^{3+} paramagnetic centers in tetrahedral clusters in $Cd_{1-x-y}Y_xGd_yF_{2+x+y}$ is simpler. Perhaps, that is why it proved possible to identify transitions in the EPR spectrum of this crystal and to find the parameters of two monoclinic and one trigonal gadolinium center [13, 14].

Determination of the orientation behavior of the EPR spectrum of $Ca_{1-x-y}Y_xGd_yF_{2+x+y}$ is intricate due to the presence of magnetically nonequivalent low-symmetry centers, whose spectra largely coincide at $\mathbf{B} \parallel \mathbf{C}_4$ but differ at an arbitrary orientation. Since lowering the symmetry of the paramagnetic centers to C_{2V} and C_S occurs due to the cationic (not nearest) neighborhood, it should be expected that the parameters of their spin Hamiltonian and, consequently, the resonance positions of the signals differ insignificantly from those of the tetragonal centers.

It is exactly the existence of similar centers that most likely causes the scatter in the principal axes of the g tensor of Er^{3+}, Tm^{3+}, and Yb^{3+} ions observed in [5–8]. This means that the spectral lines are superpositions of the transitions of weakly distorted tetragonal centers with their original angular dependences.

4. Thorough investigation of the transformation of the spectrum near the transitions of the cubic Gd^{3+} center in $Ca_{1-x-y}Y_xGd_yF_{2+x+y}$ with a change in the orientation of the magnetic field in the (Figs. 3, 4) C_4–C_2 and (Fig. 5) C_4–C_3 plane revealed the presence of weak satellites of these signals, which exhibit the orientation behavior near $\mathbf{B} \parallel \mathbf{C}_4$ similar to that of the cubic center. The positions of these satellites at $\mathbf{B} \parallel \mathbf{C}_4$ are shown in Fig. 2. The angular dependences of the measured positions of the satellites of the cubic Gd^{3+} center are indicated by the respective curves in Figs. 3, 4. The experimental points apart from the curves in Fig. 5 correspond to the positions of intense unidentified signals (Fig. 2) discussed in Section 3. Many of them change their shape considerably but retain the position in a noticeable range of orientations (Fig. 5).

At an arbitrary orientation of the magnetic field, as well as at $\mathbf{B} \parallel \mathbf{C}_3$ and $\mathbf{B} \parallel \mathbf{C}_2$, the satellite structure of the transitions of the cubic Gd^{3+} center cannot be resolved. The behavior of the satellites was determined more accurately by the analysis of the angular dependence of the second derivative of the absorption spectrum at room temperature and at 180 K. The dashed lines in Figs. 3, 4 indicating the orientation behavior of the position of the satellites were obtained by this kind of analysis.

The spectrum of one set of satellites (the possibility of the existence of other weaker and poorly resolved satellite centers cannot be excluded) can be described by the spin Hamiltonian ($S = 7/2$) with the tetragonal symmetry [21] in the coordinate system of the cubic center

$$H_{sp} = g\beta(\mathbf{BS}) + \frac{1}{3}b_{20}O_{20} + \frac{1}{60}(b_{40}O_{40} + b_{44}O_{44}) + \frac{1}{1260}(b_{60}O_{60} + b_{64}O_{64}),$$

Table 2. Possible types of clusters containing the gadolinium ion, the symmetry group, magnetic multiplicity, and orientation of the symmetry elements of the magnetic ion with respect to the crystal axes

Tetrahedral clusters			Octahedral clusters		
cluster type	symmetry (multiplicity) of the center	orientation of the symmetry elements	cluster type	symmetry (multiplicity) of the center	orientation of the symmetry elements
$[GdY_3F_{26}]^{1+}$	$C_{3V}(4)$		$[GdY_5F_{37}]^{1+}$	$C_{4V}(3)$	
			$[GdY_4MF_{37}]^0$	$C_{4V}(3)$	
$[GdY_2MF_{26}]^0$	$C_S(12)$	$\sigma \perp C_2$		$C_S(12)$	$\sigma \perp \mathbf{C}_4$
			$[GdY_3M_2F_{37}]^{1-}$	$C_{2V}(6)$	$\sigma \parallel \mathbf{C}_4$
$[GdYM_2F_{26}]^{1-}$	$C_S(12)$	$\sigma \perp C_2$		$C_S(12)$	$\sigma \perp \mathbf{C}_4$
				$C_S(12)$	$\sigma \perp \mathbf{C}_2$

Note: σ is the symmetry plane, and the superscript is the cluster charge relative to the charge of the substituted fragment of the structure.

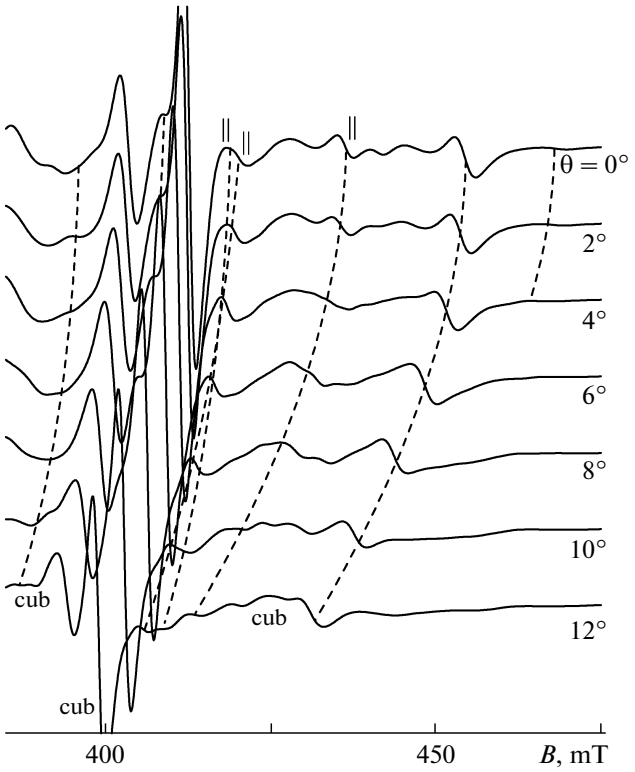

Fig. 3. High-field part of the EPR spectrum (first derivative of absorption signals) versus the polar angle in the C_4–C_2 plane at $T = 300$ K and a frequency of 9.83 GHz. The symbols || mark transitions of the quasi-cubic centers with the axis **z** || **B** at **B** || $\mathbf{C}_4$. Dashed lines indicate the orientation behavior of the signals of interest.

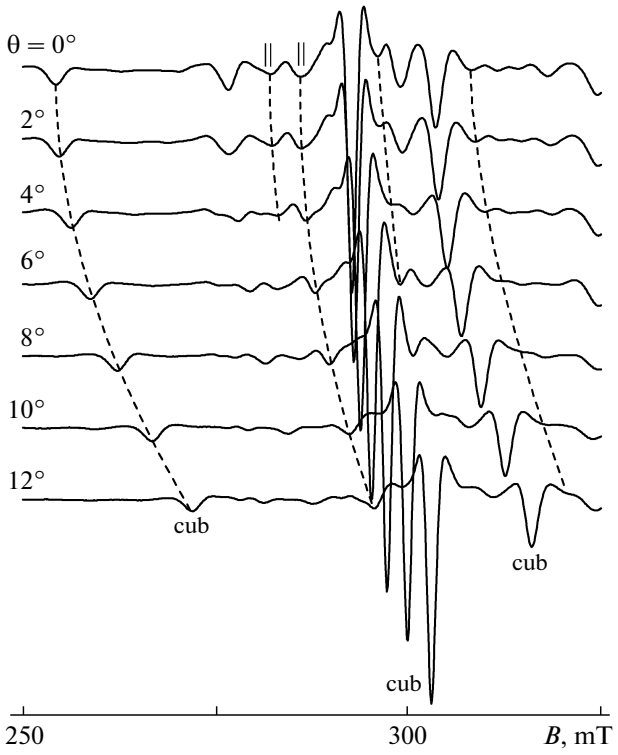

Fig. 4. Low-field part of the EPR spectrum (second derivative of absorption signals) versus the polar angle in the C_4–C_2 plane at $T = 300$ K and a frequency of 9.83 GHz.

where g is the g tensor, β is the Bohr magneton, **S** is the spin operator, b_{nm} are the fine-structure parameters, O_{nm} are the Stevens spin operators. The resulting parameters are listed in Table 3 along with the parameters of the cubic centers (for comparison). As is seen (Table 3), the main difference between the tetragonal (quasi-cubic) and cubic centers is the presence of the axial parameter b_{20} for the former ones. Imperfect agreement of the calculated curves with the experimental data in Fig. 5 is caused primarily by the errors in the resonance positions owing to overlap of the signals. For example, the satellite at 437 mT for **B** || $\mathbf{C}_4$ in Fig. 3 obviously overlaps with the unknown signal (γ in Fig. 5). The accurate measurement of the orientation behavior of the transitions with the calculated positions 242.7 and 273.3 mT for **B** || $\mathbf{C}_4$ turned out to be impossible owing to the intense signals (α and β in Fig. 5), whose positions, as well as that of the signal γ, are shown by dotted lines in Fig. 5. As indicated in Fig. 2, the signal α is the transition of the tetragonal Gd^{3+} dimer center.

It can be assumed that the discovered centers are caused by individual Gd^{3+} ions situating near the octahedral rare-earth clusters or their groups. Owing to a difference in size between the rare-earth supercluster and the substituted fragment of the fluorite structure, the nearest anionic neighborhood of such centers should quite probably form a truncated square pyramid. According to [2], the volumes of the rare-earth octahedral supercluster $\{Ca_8[Y_6F_{69}]\}$ and the matrix fragment $[Ca_{14}F_{64}]$ are ~0.59 and ~0.57 nm^3, respectively. Consequently, the dimensions of the square facets of the above pyramid are ~0.280 and ~0.276 nm.

As a result of studying the effect of uniaxial pressure on the EPR spectrum of Gd^{3+} centers in CaF_2 crystals, Newman et al. [22, 23] suggested the following relation between the parameters of the spin Hamiltonian and the coordinates of the nearest ligands, which became known as the superposition model:

$$b_{nm} = \sum_d K_{nm}(\theta_d, \phi_d)\bar{b}_n(R_d), \quad (1)$$

$$\bar{b}_n(R_d) = \bar{b}_n(R_0)(R_0/R_d)^{t_n}, \quad (2)$$

where $K_{nm}(\theta_d, \phi_d)$ is the angular structure factor, R_d, θ_d, ϕ_d are the spherical coordinates of the ligands, $R_0 = 0.237$ nm is the sum of ionic radii of the impurity ion and ligand $\bar{b}_2(R_0) = -600 \times 10^{-4}$ cm^{-1}, $t_2 = -1.2$,

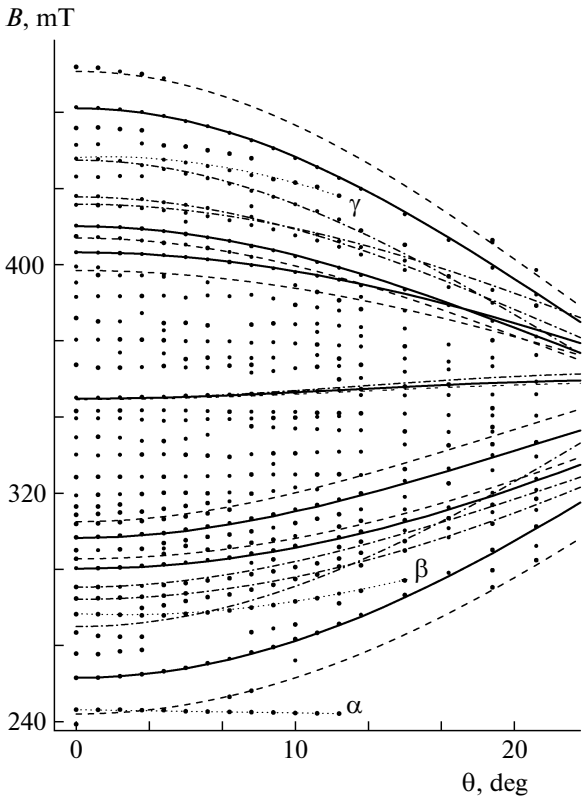

Fig. 5. Orientation behavior of the spectrum of $Ca_{1-x-y}Y_xGd_yF_{2+x+y}$ in the C_4–C_3 plane at $T = 300$ K and a frequency of 9.87 GHz. Dots are the experimental data, curves are the calculation results for (solid lines) cubic centers, (dashed lines) quasi-cubic centers with the axis $\mathbf{z} \perp \mathbf{B}$ at $\mathbf{B} \parallel \mathbf{C}_4$ and (dash-dotted lines) quasi-cubic centers with the axis $\mathbf{z} \parallel \mathbf{B}$ at $\mathbf{B} \parallel \mathbf{C}_4$.

$\bar{b}_4(R_0) = 14.9 \times 10^{-4}$ cm^{-1}, $t_4 = 7.2$ are the empirical parameters of the model.

With the use of the above expressions and constants, one can estimate the parameters of the spin Hamiltonian of the hypothetic tetragonal (quasi-cubic) center. We assume that the spherical coordinates of the ligands ($\mathbf{z} \parallel \mathbf{C}_4$) situated on the most apart facet from the rare-earth supercluster are the same as in pure CaF_2 ($R = 0.239$ nm, $\theta = 54.7°$), whereas, according to [2], the ligands situating on the opposite facet have larger parameters, $R_d = 0.241$ nm and $\theta_d = 55.1°$.

Table 3. Parameters of the spin Hamiltonian of cubic and quasi-cubic (tetragonal) Gd^{3+} centers in $Y_xCa_{1-x}F_{2+x}$ (the standard deviation f and the parameters b_{nm} are given in MHz)

Parameter	Cubic center (experiment [19])	Tetragonal center	
		experiment	calculation
g	1.991	1.991	
b_{20}	–	105 (5)	59
b_{40}	−139.2	−146 (2)	−126
b_{44}	−696	−692 (10)	−638
b_{60}	−0.3	0 (2)	
b_{64}	6	30 (25)	
f	3.4	20	

The results of the calculation of the parameters b_{20}, b_{40}, and b_{44} with the use of these coordinates and Eqs. (1), (2) are listed in Table 3. Bearing in mind the approximate character of the superposition model, a fair agreement between the experimental and calculated values can be regarded as a valuable argument in favor of our assumption on the origin of quasi-cubic (tetragonal) centers.

It should be mentioned that many transitions of tetragonal Gd^{3+}–F_i^- dimer centers are also accompanied by satellites (Fig. 2) with similar orientation behavior. Most probably, these satellite signals are caused by the tetragonal Gd^{3+}–F_i^- dimer centers situated near the cluster formations.

In contrast to $Ca_{1-x-y}Y_xGd_yF_{2+x+y}$, the spectra of yttrium- and gadolinium-doped cadmium fluoride do not exhibit the satellites of the cubic Gd^{3+} centers similar to those discussed above. A possible reason of this is presumably another way of the formation of the groups of tetrahedral clusters.

5. Electron paramagnetic resonance of yttrium- and gadolinium-doped calcium fluoride single crystals has revealed an intense spectrum. According to qualitative analysis, this spectrum can be attributed to the transitions of Gd^{3+} ions localized in octahedral clusters.

We have also detected weak satellites of the signal of a cubic Gd^{3+} center, which exhibit the orientation behavior typical for cubic centers. The spectrum of the satellites has been described by the tetragonal spin Hamiltonian with the parameters close to those of the cubic center. The estimates of the parameters of the spin Hamiltonian in the superposition approximation for a weakly deformed nearest neighborhood of an individual Gd^{3+} ion imply that the above tetragonal (quasi-cubic) centers are due to the gadolinium ions situated near the octahedral yttrium clusters or their groups.

ACKNOWLEDGMENTS

This study was supported by the Ural Federal University within the framework of the Competition of Young Scientists and the program of the Development of the Ural Federal University.

REFERENCES

1. B. P. Sobolev, *The Rare-Earth Trifluorides* (Institut d'Estudis Catalans, Barcelona, 2001), Part 2.
2. B. P. Sobolev, A. M. Golubev, and P. Herrero, Crystallogr. Rep. **48** (1), 141 (2003).
3. O. Greiss and J. M. Hashke, in *Handbook on the Physics and the Chemistry of Rare Earths*, Ed. by K. A. Gschneidner and L. R. Eiring (North-Holland, Amsterdam, 1982), p. 387.
4. D. J. M. Bevan, J. Strahle, and O. Greis, J. Solid State Chem. **44**, 75 (1982).
5. S. A. Kazanskii, Sov. Phys. JETP **62** (4), 527 (1985).
6. S. A. Kazanskii and A. I. Ryskin, Phys. Solid State **44** (8), 1415 (2002).
7. A. E. Nikiforov, A. Yu. Zakharov, M. Yu. Ugryumov, S. A. Kazanskii, A. I. Ryskin, and G. S. Shakurov, Phys. Solid State **47** (8), 1431 (2005).
8. S. A. Kazanskii, A. I. Ryskin, A. E. Nikiforov, A. Yu. Zaharov, M. Yu. Ougrumov, and G. S. Shakurov, Phys. Rev. B: Condens. Matter **72**, 014127 (2005).
9. L. A. Muradyan, B. A. Maksimov, and V. I. Simonov, Koord. Khim. **12**, 1398 (1986).
10. E. A. Sul'yanova, A. P. Shcherbakov, V. N. Molchanov, V. I. Simonov, and B. P. Sobolev, Crystallogr. Rep. **50** (2), 203 (2005).
11. E. A. Ryzhova, V. N. Molchanov, A. A. Artyukhov, V. I. Simonov, and B. P. Sobolev, Crystallogr. Rep. **49** (4), 591 (2004).
12. N. I. Sorokin, E. A. Sul'yanova, I. I. Buchinskaya, and B. P. Sobolev, Crystallogr. Rep. **50** (4), 695 (2005).
13. V. A. Vazhenin, A. P. Potapov, A. D. Gorlov, V. A. Chernyshev, S. A. Kazanskii, and A. I. Ryskin, Phys. Solid State **48** (4), 686 (2006).
14. V. A. Vazhenin, V. A. Chernyshev, V. B. Guseva, A. P. Potapov, and M. Yu. Artyomov, Phys. Solid State **50** (3), 425 (2008).
15. E. A. Sul'yanova, V. N. Molchanov, and B. P. Sobolev, Crystallogr. Rep. **53** (4), 565 (2008).
16. B. P. Sobolev, A. M. Golubev, L. P. Otroshchenko, V. N. Molchanov, R. M. Zakolyukin, E. A. Ryzhova, and P. Herrero, Crystallogr. Rep. **48** (6), 944 (2003).
17. L. K. Aminov, R. Yu. Abdulsabirov, S. L. Korableva, I. N. Kurkin, S. P. Kurzin, A. G. Ziganshin, and S. B. Orlinskii, Appl. Magn. Reson. **29**, 561 (2005).
18. L. K. Aminov and I. N. Kurkin, Phys. Solid State **51** (4), 741 (2009).
19. V. A. Vazhenin, A. P. Potapov, A. D. Gorlov, A. E. Nikiforov, S. A. Kazanskii, A. I. Ryskin, Phys. Solid State **47** (8), 1454 (2005).
20. K. Zdansky and A. Edgar, Phys. Rev. B: Solid State **3**, 2133 (1971).
21. C. A. Al'tshuler and B. M. Kozyrev, *Electron Paramagnetic Resonance* (Academic, New York, 1964; Nauka, Moscow, 1972), p. 121.
22. D. J. Newman and W. Urban, J. Phys. C: Solid State Phys. **5**, 3101 (1972).
23. A. Edgar and D. J. Newman, J. Phys. C: Solid State Phys. **8**, 4023 (1975).

Translated by A. Safonov